Biochimica et Biophysica Acta 1834 (2013) 1468–1473

Contents lists available at SciVerse ScienceDirect

Biochimica et Biophysica Acta

journal homepage: www.elsevier.com/locate/bbapap

Ostreopexin: A hemopexin fold protein from the oyster mushroom, *Pleurotus ostreatus*

Katja Ota [a], Miha Mikelj [a], Tadeja Papler [a], Adrijana Leonardi [b], Igor Križaj [b,c,d], Peter Maček [a,*]

[a] Department of Biology, Biotechnical Faculty, University of Ljubljana, Večna pot 111, SI-1000 Ljubljana, Slovenia
[b] Jožef Stefan Institute, Jamova 39, SI-1000 Ljubljana, Slovenia
[c] Department of Chemistry and Biochemistry, Faculty of Chemistry and Chemical Technology, University of Ljubljana, Aškerčeva 5, SI-1000 Ljubljana, Slovenia
[d] Centre of Excellence for Integrated Approaches in Chemistry and Biology of Proteins, Jamova 39, SI-1000 Ljubljana, Slovenia

ARTICLE INFO

Article history:
Received 26 February 2013
Received in revised form 27 March 2013
Accepted 29 March 2013
Available online 6 April 2013

Keywords:
Albumin-2
Fungus
Hemin
Hemopexin-like protein
Iron-protoporphyrin (IX)
HX-repeat

ABSTRACT

Proteins with hemopexin repeats are widespread in viruses, prokaryotes and eukaryotes. We report here for the first time the existence of a protein in fungi with the four-bladed β-propeller fold that is typical for hemopexin-like proteins. This protein was isolated from the edible basidiomycetous fungus *Pleurotus ostreatus* and is named ostreopexin. It binds to Ni^{2+}-NTA-agarose, and is structurally and functionally very similar to PA2 albumins isolated from legume seeds and the hemopexin fold protein from rice. Like these plant proteins, ostreopexin shows reversible binding to hemin with moderate affinity, but does not bind to polyamines. We suggest that ostreopexin participates in intracellular management of metal (II or III)-chelates.

1. Introduction

Proteins of the hemopexin family (Pfam: PF00045), which was previously known as the "pexin family" [1], have various numbers of hemopexin-like repeats (HX-repeats), and they are widely distributed among organisms. The heme-binding glycoprotein hemopexin, vitronectin and extracellular matrix metalloproteinases are the best known representatives of HX-repeat proteins [2–5]. In plants, several hemopexin-like proteins have been discovered in legumes, and most recently in rice [6–11]. These proteins have been suggested to have roles in polyamine metabolism and in the protection from heme-induced oxidative stress in legumes [9,11], and to participate in chlorophyll degradation in rice [11]. The large majority of the hemopexin family members are putative proteins, including photopexins A and B from *Photorhabdus fluorescens*, the first bacterial proteins predicted to have HX-repeats [12]. Such proteins have also been predicted for fungi; e.g., in *Uncinocarpus reesii*, *Coccidioides immitis*, *Coccidioides posadasii* and *Postia placenta*. Search of the Joint Genome Institute genomic databases [13] reveals a putative protein (JGI: Protein ID: 1113759) with HX-repeats also in the edible oyster mushroom *Pleurotus ostreatus*. However, none of these have been described at the protein level.

Here, we present the isolation and identification of a native protein from *P. ostreatus* that has four HX-repeats, which we have named ostreopexin (Opx). We detected this ~26 kDa protein as it co-eluted anomalously with another mushroom protein, ostreolysin A, in size-exclusion chromatography [14]. Partial amino-acid sequencing and its tight binding to Ni^{2+}-nitrilotriacetic acid (NTA)-agarose suggest that Opx might be a bivalent-metal-binding protein. Functional studies using recombinant Opx reveal here for the first time that fungi can produce four-bladed hemopexin-like proteins that are very similar to orthologs from plants. We show that Opx binds hemin but not polyamines.

2. Material and methods

2.1. Materials

The *Nde*I and *Xho*I restriction enzymes, Rapid DNA ligation kits, GeneJET™ PCR purification kits; GeneJET™ gel extraction kits, TransformAid™ bacterial transformation kits, GeneJET™ plasmid miniprep kits, and PageRuler™ prestained protein ladder were from Fermentas (Germany). Thrombin and the plasmid pET were

Abbreviations: 3D, three-dimensional; BSA, bovine serum albumin; ESI-MS, electrospray ionization mass spectrometry; H_6, hexahistidine; Hn.Cl, hemin chloride; HX-repeat, hemopexin-like repeat; LC–MS/MS, liquid chromatography–mass spectrometry; nOpx, native ostreopexin; NTA, nitrilotriacetic acid; Opx, ostreopexin; PBS, phosphate-buffered saline; rOpx, recombinant ostreopexin; TBS, Tris-buffered saline; TFA, trifluoroacetic acid

* Corresponding author at: Department of Biology, University of Ljubljana, Večna pot 111, SI-1000 Ljubljana, Slovenia. Tel.: +386 1 3203395; fax: +386 1 2573390.
E-mail addresses: katja.ota@bf.uni-lj.si (K. Ota), tadeja.papler@gmail.com (T. Papler), adrijana.leonardi@ijs.si (A. Leonardi), igor.krizaj@ijs.si (I. Križaj), peter.macek@bf.uni-lj.si (P. Maček).

1570-9639/$ – see front matter © 2013 Elsevier B.V. All rights reserved.
http://dx.doi.org/10.1016/j.bbapap.2013.03.027

from Novagen (Millipore, USA). Oligonucleotide primers and the gene coding for rOpx-H_6 were synthesized by MWG Operon (Germany). PD-10 desalting columns, Mono Q anion-exchange columns and Biacore C5 chips were from GE Healthcare (Sweden). Ni^{2+}-NTA-agarose was from Qiagen (USA). Protein concentrations were determined using Pierce BCA protein assay reagents (Thermo Scientific, USA). Protein sizes and purities were determined using SDS-PAGE, with homogenous 12% polyacrylamide gels. Proteins were stained with Coomassie blue. Hemin chloride (Hn.Cl) and other materials and analytical grade chemicals were from Sigma-Aldrich and Merck (Germany). The stock solution of 1 mM Hn.Cl was prepared in 10 mM NaOH, kept in the dark at 4 °C, and used within 24 h [15], to prepare the fresh 100 μM Hn.Cl in 140 mM NaCl, 20 mM Tris–HCl, pH 7.4 (Tris-buffered saline; TBS) or 20 mM $NaH_2PO_4 \cdot 2H_2O$, 20 mM Na_2HPO_4, 140 mM NaCl, pH 7.4 (phosphate-buffered saline; PBS), respectively. *P. ostreatus* (strain Plo5) was from the ZIM collection of the Biotechnical Faculty, University of Ljubljana (Slovenia).

2.2. Partial isolation of native ostreopexin

Native (n)Opx was partially purified as a contaminant protein during isolation of ostreolysin A [14]. Briefly, a total protein extract from fresh primordia and young basidiomata of the mushroom *P. ostreatus* was fractionated using solid ammonium sulfate. The protein fraction that precipitated between 35% and 60% ammonium sulfate saturation was dissolved in 50 mM Tris–HCl, pH 8.0, applied to size-exclusion chromatography on a Sephadex G-75 column at 4 °C, and eluted with 50 mM Tris–HCl, pH 8.0. The protein peak (P3, Supplementary Fig. S1) was analyzed by SDS-PAGE, and an unknown protein with a molecular mass of ~26 kDa was characterized by internal Edman micro-sequencing, electro-spray ionization mass spectrometry (ESI-MS), and liquid chromatography–mass spectrometry (LC–MS/MS) amino-acid sequencing.

2.3. Purification of native ostreopexin on Ni^{2+}-NTA-agarose

We then took advantage of the affinity of bivalent-metal-binding proteins for Ni^{2+}-NTA-agarose [16]. Cell extracts of *P. ostreatus* were prepared by homogenization of fresh primordia and young basidiomata (10 g) in 10 mL ice-cold extraction buffer (50 mM NaH_2PO_4, 300 mM NaCl, 1 mM phenylmethylsulfonyl fluoride, pH 7.0). The homogenate was centrifuged at 26,323 ×g at 4 °C for 30 min. One milliliter of Ni^{2+}-NTA-agarose was added to the extract, which was mixed gently for 1 h at 4 °C, and then packed into a column. The column was washed with the extraction buffer until a stable baseline was seen. The Ni^{2+}-NTA-bound proteins were eluted step-wise by decreasing the pH of the extraction buffer used for the elution to 5.9 and then to 4.5. The pH of the collected 1 mL fractions was adjusted to 7.0 with the addition of 1 M Tris–HCl buffer, pH 9.0. Alternatively, Ni^{2+}-NTA-bound proteins were desorbed by using 300 mM imidazole in the extraction buffer. For SDS-PAGE analysis of the fractions, the proteins were concentrated with trichloroacetic acid precipitation. The single protein of ~26 kDa that eluted at pH 4.5 was analyzed by ESI-MS and LC–MS/MS.

2.4. Expression and purification of recombinant proteins

The amino-acid sequence of the predicted HX-repeat protein (JGI: Protein ID: 1113759) was taken from the *P. ostreatus* genome assembly PC15 v2.0 [13], reverse translated, and adapted for expression as recombinant (r)Opx in *Escherichia coli*. The gene coding for the consensus nOpx (see Supplementary Fig. S2) was cloned into the pET21c(+) vector via the *Nde*I and *Xho*I sites, to obtain an expression construct with a C-terminal hexahistidine (H_6)-tag preceded by a linker, and a thrombin cleavage site. The nucleic acid sequence of the forward primer was: 5′-AAAAACATATGACCCCAGCTCGTGCGGCA-3′ (*Nde*I site underlined), and the reverse primer: 5′-AAAAAACTCGAG**GCTGCCGCGCGGAACCAG***G CCGCTGCTTTTGCCTTCGCTGCC*ATAAAAGCCCGCTTGTTTCAA-3′ (*Xho*I site underlined; linker region in italics, and thrombin cleavage site in bold). The nucleotide sequences were analyzed by MWG Operon.

C-terminally H_6-tagged rOpx (rOpx-H_6) was expressed in an *E. coli* strain BL21(DE3), transformed with the pET21c(+)-Opx vector, as a soluble product (yield ~2 mg/L culture), and purified on Ni^{2+}-NTA-agarose according to standard protocols provided by Qiagen. For functional studies, the H_6-tag was removed with thrombin at 1 U/mg protein at 22 °C for 16 h. Prior to cleavage, the Ni^{2+}-NTA elution buffer (300 mM imidazole, 300 mM NaCl, 50 mM NaH_2PO_4. $2H_2O$, pH 8.0) was exchanged for thrombin cleavage buffer (20 mM Tris–HCl, 150 mM NaCl, 2.5 mM $CaCl_2$, pH 8.4) on a PD-10 desalting column. After the thrombin cleavage, the sample buffer was exchanged for 20 mM Tris–HCl, pH 8.0, to purify the rOpx on a Mono Q anion-exchange column. The protein was eluted with a 0–100 mM NaCl gradient in the same buffer.

2.5. Protein primary structure analysis

Edman degradation of the intact nOpx from size-exclusion chromatography that had been electro-transferred from the SDS-PAGE gel to a polyvinylidene difluoride membrane (Millipore) was not effective, most likely due to a blocked terminal amino group. Therefore, the protein was isolated first on a C_4-RP HPLC column using a 0% to 90% acetonitrile gradient in 0.1% (v/v) TFA, and then hydrolyzed using sequencing grade trypsin (Sigma, USA). The resulting tryptic peptides were separated on a C_8-RP HPLC column using a 0% to 90% acetonitrile gradient in 0.1% (v/v) TFA. The four most abundant peptides were N-terminally sequenced by automated Edman degradation on a Procise 492A protein sequencing system (Applied Biosystems).

2.6. ESI–MS and LC–MS/MS amino acid sequencing

The proteins were analyzed using a 1200 series HPLC-Chip-LC/MSD Trap XCT Ultra mass spectrometer (Agilent Technologies, Germany) and a MALDI-TOF UltrafleXtreme III mass spectrometer (Bruker, USA). Prior to MS analysis, the proteins were additionally purified on a C_4-RP HPLC column using a 0% to 90% acetonitrile gradient in 0.1% (v/v) TFA, reduced, carboxamidomethylated, and fragmented with proteomics grade trypsin (Sigma, USA). Mass spectrometry data were analyzed using Spectrum Mill software Rev A.03.03.084 SR4 (Agilent Technologies, Santa Clara, CA, USA) on the NCBI protein database and the JGI raw genome data (*P. ostreatus* PC15 v2.0) [13]. To align the amino-acid sequences, the on-line ClustalW [17] or MAFFT software [18] was used.

2.7. Modeling of three-dimensional structure

Homology modeling of nOpx and searching for similar three-dimensional (3D) structures were performed with on-line I-TASSER [19], and the figures were rendered using CHIMERA [20].

2.8. Protein–hemin interactions

Interactions of hemin with rOpx or with bovine serum albumin (BSA) as the control, were studied using UV/VIS absorption, steady-state fluorescence spectroscopy, and surface plasmon resonance refractometry.

The absorption spectra (290–480 nm) of both rOpx and BSA (20 μM each, in PBS) before and 2 min after the addition of the final 10 μM Hn.Cl were recorded in a 1-cm light path quartz cuvette using a Shimadzu UV2101PC UV–VIS scanning spectrophotometer.

Steady-state fluorescence measurements were performed on a Jasco FP750 spectrofluorometer in a thermostated cell holder at 20 °C, equipped with a magnetic stirrer. The emission and excitation bandwidths were set to 10 nm. The sample volume was 1.5 mL in a 1-cm path length quartz cuvette. Intrinsic fluorescence of rOpx and BSA (2 μM, in 140 mM NaCl, 20 mM Tris–HCl, pH 7.4) was measured by selective exciting of the fluorescence of tryptophan residues at 295 nm wavelength. The emission spectra were recorded in the 300 nm to

450 nm range, before and after 10 min incubations with Hn.Cl (2, 4, 10 μM). In fluorimetric titration experiments, aliquots of 100 μM Hn.Cl in PBS were added to 2 μM rOpx or BSA, to reach final concentrations of 0.2 μM to 18.9 μM Hn.Cl. The fluorescence emission intensity was monitored at a wavelength of 330 nm, at 20 °C. The final Hn.Cl concentrations were corrected for each volume increment. The Hn.Cl quenching constant was evaluated using the Stern–Volmer plot [21]:

$$F_0/F_{corr} = 1 + K_{SV} * [Q] \quad (1)$$

where, F_0 and F_{corr} are the fluorescence intensities of the proteins in the absence and presence of a given concentration of the quencher, [Q]. F_{corr} is the fluorescence intensity corrected for the inner filter effect, and K_{SV} is a Stern–Volmer quenching constant. With respect to the geometry of the measuring cell, the fluorescence intensity was corrected for primary and secondary inner filter effects according to Lakowicz [21–23] as:

$$F_{corr} = F_{obs} * 10^{(A_{295}+A_{330}/2)/2} \quad (2)$$

where, F_{obs} is the observed fluorescence upon titration of the protein with Hn.Cl at a wavelength of 330 nm, and A_{295} and A_{330} are the absorbances of Hn.Cl at 295 nm (protein excitation wavelength) and 330 nm (fluorescence emission wavelength), respectively.

The kinetics of the interactions were monitored on Biacore X and Biacore T100 surface-plasmon-resonance-based refractometers, and the data were processed using the BIAevaluation software (GE Healthcare, Sweden). rOpx or BSA was coupled to a CM5 chip at up to 3000 RU using a standard N-hydroxysuccinimide/N-ethyl-N′-[3-dimethyl aminopropyl]-carbodiimide coupling procedure, as recommended by the manufacturer. Hn.Cl solutions at 0.2 μM to 1.0 μM in PBS were injected at a flow rate of 30 μL/min for 60 s in PBS as a running buffer, at 25.0 °C. Nonspecific interactions were minimized by adding 0.005% P20 surfactant to the running buffer. Sensorgrams were corrected for the reference flow-cell response (nonderivatized surface), and fitted to standard kinetic models provided by the BIAevaluation package. Similarly, as described above, we additionally checked the interactions of the immobilized rOpx with polyamines as analytes: spermidine, spermine, putrescine and cadaverine (all at 0.2 mM or 2 mM, in PBS).

3. Results and discussion

SDS-PAGE analysis of the peak P3 from the size-exclusion chromatography of the dissolved 35% to 60% ammonium sulfate protein precipitate resulted in a ~26 kDa protein band (Supplementary Fig. S1, nOpx) and the ~16 kDa ostreolysin A. N-terminal amino-acid sequencing of the intact ~26 kDa protein that had been electro-transferred to polyvinylidene difluoride membranes failed, probably due to a blocked N-terminal amino group. Hence, this protein with an ESI–MS-determined molecular mass of 25,101.0 Da was isolated on a C_4-RP HPLC column and fragmented with trypsin, to enable micro-sequencing of the internal peptides. Of note, nOpx is highly resistant to trypsin, so that even after an 18 h incubation, and with additions of fresh trypsin, we could still detect some intact protein on SDS-PAGE (not shown). The *P. ostreatus* total protein extract on Ni^{2+}-NTA-agarose resulted in the tight binding of a single protein (Fig. 1). This behavior is typical for proteins with affinity for chelated bivalent metal ions [16]. The eluted protein had a molecular mass of 25,101.0 Da, which is identical to that of nOpx from the size-exclusion chromatography. The identity of the protein was furthermore supported by partial LC–MS/MS sequencing (Supplementary Fig. S2). Based on these sequence data and the identical molecular mass of nOpx obtained from both size-exclusion and metal-affinity chromatography, we derived a proposed consensus amino-acid sequence for native ostreopexin (Supplementary Fig. S2, nOpx (b)). This consensus sequence is assumed to be shorter than that translated from the nucleotide sequence, and therefore the isolated native nOpx might be a mature, post-translationally processed form. Hence, we constructed recombinant Opx that was C-terminally tagged with a linker peptide, thrombin cleavage site, and a H_6 sequence (Supplementary Fig. S2, rOpx-H_6 (c)).

The rOpx-H_6 was expressed in *E. coli* as a soluble protein with a molecular mass of 27,132.6 Da, which is lower than the expected mass for this protein (27,605.9 Da). We suggest that this difference might originate from the bacterial processing of the protein. After cleavage of the H_6-tag from rOpx-H_6, we used the purified rOpx for functional studies (Fig. 1b and Supplementary Fig. S2 (d)). We assumed that the recombinant protein most likely retained the functionalities of the native form, as it exhibited a similar behavior; i.e., retention on Sephadex columns, Ni^{2+}-NTA-agarose binding, and resistance to trypsin degradation. In contrast to LS-24, a plant hemopexin-like protein from *Lathyrus sativus* that is similar to nOpx, no dimerization in solution was observed for nOpx or rOpx.

The amino-acid sequence analysis revealed that nOpx is most similar to the predicted hemopexin-like proteins from the fungi *U. reesii* (38% identity, E-value 1.0×10^{-53}), *C. posadasii* (38%, 2.0×10^{-52}) and *C. immitis* (38%, 3.0×10^{-52}), and also to plant representatives from *Vigna radiata* (35%, 1.0×10^{-33}), *Pisum sativum* (34%, 2.0×10^{-33}) and *L. sativus* (33%, 1.0×10^{-30}) (see also sequence alignment in Supplementary Fig. S2). In the 3D structural model of nOpx (Supplementary Fig. S3), four HX-repeats are folded into a β-propeller domain with four blades, similar to other proteins of the hemopexin superfamily. The nOpx modeled 3D structure is most similar to the crystal structures of the plant hemopexin-like proteins from *Vigna unguiculata* (PDB ID: 3OYO) [9] with a RMSD Cα of 1.18 Å, and *L. sativus* (PDB ID: 3LP9) [8] with a RMSD of 1.20 Å. This supports the observation that the β-propeller fold is conserved in a large number of proteins, although their primary structures can differ significantly [24,25].

Proteins with the four-bladed β-propeller fold that forms the hemopexin domain appear to have evolved to perform a variety of functions [1,24,25]. Hemopexin itself is a plasma glycoprotein that is built of two HX-domains that are connected by a linker region. This region and the metal-binding residues located between blades can bind heme tightly, and hemopexin is thus a key player in the sequestering of toxic extracellular iron protoporphyrins [5,26]. Zinc-dependent metalloproteinases are the major subgroup of the hemopexin superfamily. In these enzymes, HX-domains that are combined with other domains increase the functional versatility of the proteins. Their most prominent and pivotal role is the proteolytic processing of the extracellular matrix, which has many physiological implications [3]. In these zinc-dependent metalloproteinases, C-terminally located HX-domains participate in interactions with substrates and inhibitors [2,3,27]. In vitronectin, another plasma protein, combination of four HX-domains with a somatomedin

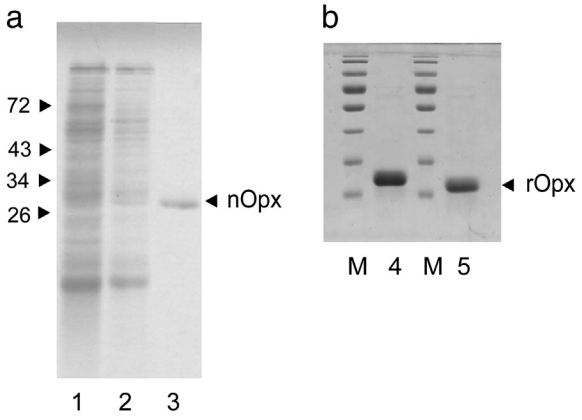

Fig. 1. Representative SDS-PAGE of nOpx, rOpx-H_6 and rOpx eluted from Ni^{2+}-NTA-agarose. (a) Lane 1, total protein extract; lane 2, protein not adsorbed to Ni^{2+}-NTA-agarose (flow-through); lane 3, nOpx from *P. ostreatus* eluted at pH 4.5. (b) Lane 4, rOpx-H_6; lane 5, rOpx (after removal of H_6 tag); M, molecular mass markers, as indicated on left of (a) in kDa.

domain, RGD motif, and heparin binding domains, enables this protein to operate multi-functionally [4,28]. In contrast to these vertebrate proteins, the function and biological roles of bacterial, fungal and plant hemopexin-like proteins remain little known. Recently, hemopexin-like proteins isolated from legume seeds were shown to bind various ligands. The garden pea (*P. sativum*) PA2 protein has been reported to bind thiamine [29], while a very similar protein from *Lens culinaris* binds both thiamine and hemin [10]. The chickpea (*Cicer arietinum*) seed albumin PA2 can interact with hemin [6]. The grass pea (*L. sativus*) protein LS-24 can bind spermine or hemin mutually [8], but CP4 from cow pea (*V. unguiculata*), a protein with a 41% sequence similarity to LS-24, interacts with spermine only [9]. Moreover, the binding of hemin has also been reported for a rice plant (*Oryza sativa*) protein, OsHFP, which has a 3D structure very similar to LS-24 [11].

Our finding that nOpx binds tightly to Ni^{+2}-NTA-agarose columns suggested that it is a bivalent-metal-binding protein. Indeed, further assays have shown that rOpx can interact with hemin, but in contrast to LS-24 and CP4, rOpx gave no surface plasmon resonance response with polyamines (Supplementary Fig. S4). The first line of evidence for an rOpx–hemin interaction came from increased absorbance and the shift of the Soret spectral band of hemin (Fig. 2), which is typical for metalloporphyrins [30]. Here, we used BSA as a reference protein, which is well-known to bind hemin [31,32]. The rOpx-induced increase in hemin absorbance is lower than that compared to BSA, which suggests that affinity of rOpx for hemin is lower than that of BSA.

Next we explored the hemin binding characteristics in more detail using quenching of the protein tryptophan fluorescence by hemin, and surface plasmon resonance kinetics analysis of the protein–hemin interaction. In agreement with the absorbance data, the hemin quenching of BSA was more efficient compared to rOpx (Fig. 3). The fluorescence emission spectra and their wavelength maxima (λ_{max}) in Fig. 3a suggest that two BSA tryptophan residues are more solvent-exposed, and are also more efficiently quenched by hemin than the same four in rOpx. We obtained a virtually linear Stern–Volmer plot only after correction of fluorescence intensity for inner filter effects (Fig. 3b). Using uncorrected data, we observed that hemin concentrations even above ~1 μM produced significant upward curving of the Stern–Volmer plot, as has been observed already before for serum albumins [32]. This might explain why our quenching constant, K_{SV}, of 4.75×10^4 L/mol determined for BSA is markedly smaller than that of 1.4×10^6 L/mol determined previously for BSA [32], although this was reported for uncorrected fluorescence intensities. Comparably, our K_{SV} of 2.62×10^4 L/mol determined for rOpx titration is lower, but in the range of that of BSA. We suggest that both values for K_{SV} are largely accounted for by a static quenching component that results from binding of hemin to the protein probes, with little due to dynamic hemin quenching of the tryptophan residues [21].

Steady-state fluorimetric titration is one of the most used techniques for the evaluation of the binding of small ligands to proteins. However, determination of reliable binding constants can be complex, and this can be hampered by a variety of factors (reviewed in [22]). This is also true here, primarily due to the solubility properties of hemin, and to unknown (non)equivalent binding sites/protein molecule, or even to various classes of binding sites [22]. Specifically, when hemin and other metalloprotoporphyrins IX are above ~1 μM in solution, it is well-known that they form dimers, and then they aggregate to form micelles if their concentration exceeds 4 μM [15]. These dimerization and aggregation processes might influence the binding of the metalloporphyrins to proteins, as has been shown for hemopexin and other serum proteins, including albumin. This thus substantially complicates any postulation of binding models and any determination of kinetics and binding parameters [30,31]. However, if all of these

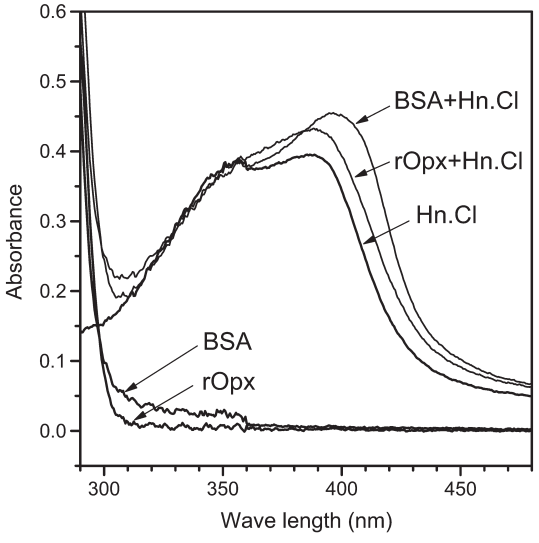

Fig. 2. Absorption spectra of hemin.chloride (Hn.Cl), rOpx, BSA, and Hn.Cl combined with rOpx or BSA (as indicated). The proteins (20 μM) and Hn.Cl (10 μM) were in phosphate buffered saline, pH 7.4.

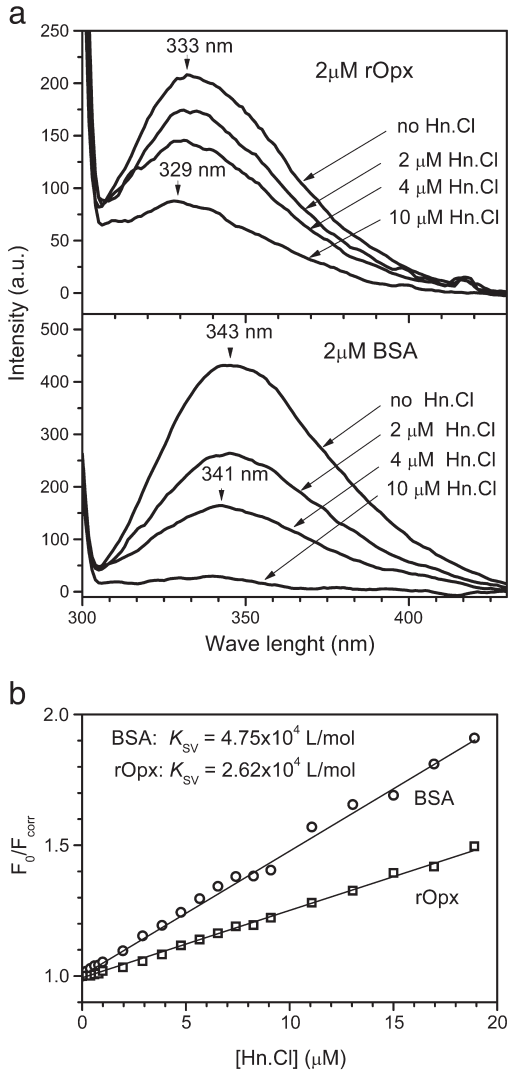

Fig. 3. Quenching of tryptophan emission fluorescence of rOpx and BSA. (a) Uncorrected fluorescence spectra of 2 μM rOpx (top) and 2 μM BSA (bottom) in 140 mM NaCl, 20 mM Tris–HCl, pH 7.4, at 20 ± 1 °C, with quenching by hemin.chloride (Hn.Cl) at indicated concentrations. Arrowheads indicate wavelength maxima (λ_{max}). (b) Stern–Volmer plot for Hn.Cl quenching of 4 μM rOpx and 4 μM BSA at 20 ± 1 °C. Excitation wave-length was 295 nm.

constraints are ignored, and with the assumption that the contribution of the dynamic quenching component is small, our fluorimetric titration will result in an apparent dissociation constant of 38 μM for the hemin–rOpx interaction. This estimated value is comparable to those determined for hemin interactions with the *C. arietinum* [6] and *L. culinaris* [10] PA2 proteins: 36 μM and 32 μM, respectively.

To reduce the ambiguities discussed above, <1 μM hemin was used in the surface plasmon resonance investigations. The fitting of real-time kinetics curves revealed that for the BSA–hemin interaction, neither 1:1 binding nor other standard kinetics models can be applied (Fig. 4). We suggest that BSA might have more binding sites for hemin, as already reported for a variety of other BSA ligands [22]. Fitting of the hemin interaction with rOpx resulted in a bivalent-ligand-binding model with high statistical significance ($\chi^2 = 0.691$). These kinetics predict that one hemin can bind two rOpx molecules with different affinities. Only the first association constant could be calculated, as 3.82×10^5 L/mol (K_d ~2.62 μM). Our estimate of the rOpx dissociation constant for hemin, as K_d ~2.62 μM, appears lower than those determined for the PA2 proteins. However, the hemin: protein binding stoichiometry of ~1:2 found for these legume proteins is similar to that of the hemin interaction with rOpx. Of note, despite a lower affinity for hemin, the mode of the hemin interaction with rOpx and the legume proteins resembles that of hemin binding to hemopexin to some extent. Hemopexin has a high affinity hemin binding site located between two four-bladed β-propeller domains and the interdomain linker [33].

Compared to other hemin-binding proteins, like hemopexin [34], glutathione transferase [35], myosins [36] and β-lactoglobulin [37], the hemin affinity for rOpx appears considerably lower. However, in addition to iron, other metal (II or III) chelates remain as putative ligands of these fungal hemopexin-like proteins as found for hemopexin in the example [38,39]. Our observation that nOpx binds tightly to Ni^{2+}-NTA-agarose supports this suggestion.

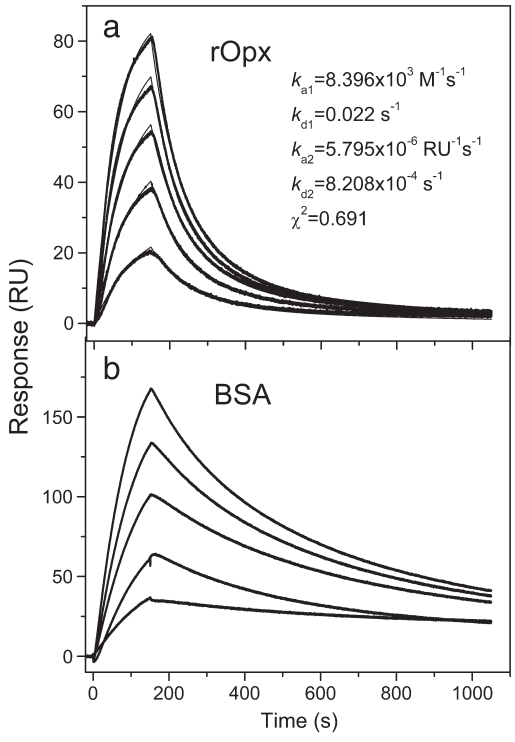

Fig. 4. Sensorgrams of rOpx (a) and BSA (b) interactions with Hn.Cl (0.2, 0.4, 0.6, 0.8 and 1.0 μM in phosphate buffered saline, pH 7.4). Hn.Cl was injected over rOpx or BSA that were immobilized on the CM5 chip, at a flow rate of 30 μL/min for 60 s, at 25 °C. Sensorgrams corrected for reference flow-cell response are shown as thick lines, and best fits as thin lines.

4. Conclusions

We have provided evidence here that *P. ostreatus* produces a four HX-repeat protein, named as ostreopexin, that has a moderate affinity for hemin, but not for polyamines. This single domain hemopexin-like protein is also predicted for some genomes of Ascomycota and Basidiomycota species, and it is structurally and functionally very similar to the plant hemopexin-like proteins, PA2 albumins, in legume seeds and rice.

Acknowledgements

This study was supported by the Slovenian Research Agency (grant P1-0207). We thank Dr. Marko Fonović and Robert Vidmar from the Department of Biochemistry and Molecular and Structural Biology, Jožef Stefan Institute and the Centre of Excellence for Integrated Approaches in Chemistry and Biology of Proteins, Ljubljana, Slovenia, for the MALDI TOF analysis. We thank Chris Berrie for the critical reading and linguistic revision of the manuscript, and Nina Orehar for the excellent technical help.

Appendix A. Supplementary data

Supplementary data to this article can be found online at http://dx.doi.org/10.1016/j.bbapap.2013.03.027.

References

[1] D. Jenne, K.K. Stanley, Nucleotide-sequence and organization of the human S-protein gene — repeating peptide motifs in the pexin family and a model for their evolution, Biochemistry 26 (1987) 6735–6742.
[2] H. Piccard, P.E. Van den Steen, G. Opdenakker, Hemopexin domains as multifunctional liganding modules in matrix metalloproteinases and other proteins, J. Leukoc. Biol. 81 (2007) 870–892.
[3] F.X. Gomis-Rüth, Hemopexin Domains, John Wiley & Sons, Ltd., Chichester, 2004. 631–646.
[4] B. Singh, Y.C. Su, K. Riesbeck, Vitronectin in bacterial pathogenesis: a host protein used in complement escape and cellular invasion, Mol. Microbiol. 78 (2010) 545–560.
[5] E. Tolosano, F. Altruda, Hemopexin: structure, function, and regulation, DNA Cell Biol. 21 (2004) 297–306.
[6] J. Pedroche, M.M. Yust, H. Lqari, C. Megias, J. Giron-Calle, M. Alaiz, F. Millan, J. Vioque, Chickpea PA2 albumin binds hemin, Plant Sci. 168 (2005) 1109–1114.
[7] H. Vigeolas, C. Chinoy, E. Zuther, B. Blessington, P. Geigenberger, C. Domoney, Combined metabolomic and genetic approaches reveal a link between the polyamine pathway and albumin 2 in developing pea seeds, Plant Physiol. 146 (2008) 74–82.
[8] V. Gaur, I.A. Qureshi, A. Singh, V. Chanana, D.M. Salunke, Crystal structure and functional insights of hemopexin fold protein from grass pea, Plant Physiol. 152 (2010) 1842–1850.
[9] V. Gaur, V. Chanana, A. Jain, D.M. Salunke, The structure of a hemopexin-fold protein from cow pea (*Vigna unguiculata*) suggests functional diversity of hemopexins in plants, Acta Crystallogr. F67 (2011) 193–200.
[10] A. Scarafoni, E. Gualtieri, A. Barbiroli, A. Carpen, A. Negri, M. Duranti, Biochemical and functional characterization of an albumin protein belonging to the hemopexin superfamily from *Lens culinaris* seeds, J. Agric. Food Chem. 59 (2011) 9637–9644.
[11] T. Chattopadhyay, S. Bhattacharyya, A.K. Das, M.K. Maiti, A structurally novel hemopexin fold protein of rice plays role in chlorophyll degradation, Biochem. Biophys. Res. Commun. 420 (2012) 862–868.
[12] S.J. Crennell, P.M. Tickler, D.J. Bowen, R.H. ffrench-Constant, The predicted structure of photopexin from *Photorhabdus* shows the first haemopexin-like motif in prokaryotes, FEMS Microbiol. Lett. 191 (2000) 139–144.
[13] I.V. Grigoriev, H. Nordberg, I. Shabalov, A. Aerts, M. Cantor, D. Goodstein, A. Kuo, S. Minovitsky, R. Nikitin, R.A. Ohm, R. Otillar, A. Poliakov, I. Ratnere, R. Riley, T. Smirnova, D. Rokhsar, I. Dubchak, The genome portal of the Department of Energy Joint Genome Institute, Nucleic Acids Res. 40 (2012) D26–D32.
[14] S. Berne, I. Križaj, F. Pohleven, T. Turk, P. Maček, K. Sepčić, *Pleurotus* and *Agrocybe* hemolysins, new proteins hypothetically involved in fungal fruiting, Biochim. Biophys. Acta 1570 (2002) 153–159.
[15] S.B. Brown, M. Shillcock, P. Jones, Equilibrium and kinetic studies of the aggregation of porphyrins in aqueous solution, Biochem. J. 153 (1976) 279–285.
[16] J. Porath, B. Olin, Immobilized metal affinity adsorption and immobilized metal affinity chromatography of biomaterials. Serum protein affinities for gel-immobilized iron and nickel ions, Biochemistry 22 (1983) 1621–1630.
[17] M.A. Larkin, G. Blackshields, N.P. Brown, R. Chenna, P.A. McGettigan, H. McWilliam, F. Valentin, I.M. Wallace, A. Wilm, R. Lopez, J.D. Thompson, T.J. Gibson, D.G. Higgins, Clustal W and Clustal X version 2.0, Bioinformatics 23 (2007) 2947–2948.

[18] K. Katoh, K. Misawa, K. Kuma, T. Miyata, MAFFT: a novel method for rapid multiple sequence alignment based on fast Fourier transform, Nucleic Acids Res. 30 (2002) 3059–3066.
[19] A. Roy, A. Kucukural, Y. Zhang, I-TASSER: a unified platform for automated protein structure and function prediction, Nat. Protoc. 5 (2010) 725–738.
[20] E.F. Pettersen, T.D. Goddard, C.C. Huang, G.S. Couch, D.M. Greenblatt, E.C. Meng, T.E. Ferrin, UCSF Chimera — a visualization system for exploratory research and analysis, J. Comput. Chem. 25 (2004) 1605–1612.
[21] J.R. Lakowicz, Principles of Fluorescence Spectroscopy, 3rd ed. Springer, Baltimore, 2006.
[22] E. Alarcon, A. Aspee, E.B. Abuin, E.A. Lissi, Evaluation of solute binding to proteins and intra-protein distances from steady state fluorescence measurements, J. Photochem. Photobiol. B 106 (2012) 1–17.
[23] C. Goletz, M. Wagner, A. Grübel, W. Schmidt, N. Korf, P. Werner, Standardization of fluorescence excitation–emission-matrices in aquatic milieu, Talanta 85 (2011) 650–656.
[24] C.K. Chen, N.L. Chan, A.H. Wang, The many blades of the beta-propeller proteins: conserved but versatile, Trends Biochem. Sci. 36 (2011) 553–561.
[25] V. Fülöp, D.T. Jones, β Propellers: structural rigidity and functional diversity, Curr. Opin. Struct. Biol. 9 (1999) 715–721.
[26] H.M. Baker, B.F. Anderson, E.N. Baker, Dealing with iron: common structural principles in proteins that transport iron and heme, Proc. Natl. Acad. Sci. U. S. A. 100 (2003) 3579–3583.
[27] H. Nagase, J.F. Woessner, Matrix metalloproteinases, J. Biol. Chem. 274 (1999) 21491–21494.
[28] A. Yoneda, H. Ogawa, K. Kojima, I. Matsumoto, Characterization of the ligand binding activities of vitronectin: interaction of vitronectin with lipids and identification of the binding domains for various ligands using recombinant domains, Biochemistry 37 (1998) 6351–6360.
[29] S. Adamek-Świerczyńska, A. Kozik, Multiple thiamine-binding proteins of legume seeds. Thiamine-binding vicilin of *Vicia faba* versus thiamine-binding albumin of *Pisum sativum*, Plant Physiol. Biochem. 40 (2002) 735–741.
[30] E. Gibbs, W.R. Skowronek, W.T. Morgan, U. Mullereberhard, R.F. Pasternack, Reactions of water-soluble metalloporphyrins with the serum-protein, hemopexin, J. Am. Chem. Soc. 102 (1980) 3939–3944.
[31] R.F. Pasternack, E.J. Gibbs, E. Hoeflin, W.P. Kosar, G. Kubera, C.A. Skowronek, N.N. Wong, U. Muller-Eberhard, Hemin binding to serum proteins and the catalysis of interprotein transfer, Biochemistry 22 (1983) 1753–1758.
[32] D. Silva, C.M. Cortez, S.R.W. Louro, Chlorpromazine interactions to sera albumins: a study by the quenching of fluorescence, Spectrochim. Acta A Mol. Biomol. Spectrosc. 60 (2004) 1215–1223.
[33] M. Paoli, B.F. Anderson, H.M. Baker, W.T. Morgan, A. Smith, E.N. Baker, Crystal structure of hemopexin reveals a novel high-affinity heme site formed between two β-propeller domains, Nat. Struct. Mol. Biol. 6 (1999) 926–931.
[34] Z. Hrkal, Z. Vodrážka, I. Kalousek, Transfer of heme from ferrihemoglobin and ferrihemoglobin isolated chains to hemopexin, Eur. J. Biochem. 43 (1974) 73–78.
[35] A.M. Caccuri, A. Aceto, F. Piemonte, C. Di Ilio, N. Rosato, G. Federici, Interaction of hemin with placental glutathione transferase, Eur. J. Biochem. 189 (1990) 493–497.
[36] V. Bhoite-Solomon, G. Kessler-Icekson, N. Shaklai, Association of iron-protoporphyrin-IX (hemin) with myosins, FEBS Lett. 266 (1990) 9–12.
[37] E. Dufour, M.C. Marden, T. Haertlé, β-Lactoglobulin binds retinol and protoporphyrin IX at two different binding sites, FEBS Lett. 277 (1990) 223–226.
[38] M.R. Mauk, F.I. Rosell, B. Lelj-Garolla, G.R. Moore, A.G. Mauk, Metal ion binding to human hemopexin, Biochemistry 44 (2005) 1864–1871.
[39] F.I. Rosell, M.R. Mauk, A.G. Mauk, pH- and metal ion-linked stability of the hemopexin–heme complex, Biochemistry 44 (2005) 1872–1879.

Supplementary Material

Ostreopexin: A hemopexin fold protein from the oyster mushroom *Pleurotus ostreatus*

Katja Ota, Miha Mikelj, Tadeja Papler, Adrijana Leonardi, Igor Križaj, and Peter Maček

Supplementary figure captions

Figure S1. Sephadex G-75 size-exclusion chromatography of the *P. ostreatus* 35% to 60% ammonium sulphate protein fraction. V_e and V_t are the elution volume and total column volume, respectively. Inset: Representative SDS-PAGE on 12% polyacrylamide gel, stained with Coomassie blue. Lane 1, proteins from 35% to 60% ammonium sulphate fraction; lane P3, peak fraction from chromatography, as indicated; M, molecular mass marker (in kDa); nOpx, native ostreopexin; nOlyA, ostreolysin A.

Figure S2. Identification of the *P. ostreatus* native hemopexin-repeat protein (nOpx). **(a, b)** Amino-acid sequence alignments. **(a)** Edman_pept_nOpx(a), tryptic peptides through internal Edman micro-sequencing of nOpx protein from Sephadex G-75. Pleos_jgi_pHX/nOpx(a) and Pleos_jgi_pHX/nOpx(b), nOpx protein from Sephadex G-75 and Ni^{2+}-NTA chromatography, respectively, showing matching of MS/MS peptides (underlined) with the amino-acid sequence of *P. ostreatus* predicted protein Pleos_jgi_pHX (not shown) (jgi|PleosPC15_2|1113759|estExt_Genemark1.C_080166, Protein ID 1113759). Also shown: sequences of predicted HX-repeat containing proteins from the fungi *Uncinocarpus reesii* (UniProt: C4JWF3) and *Coccidioides posadasii* (UniProt: E9DA27), and albumin-2 from the plants *Pisum sativum* (UniProt: P08688) and *Lathyrus sativus* (UniProt: D4AEP7). **(b)** Consensus amino acid sequence of nOpx. Asterisks, identical residues. The four HX-repeat sequences are in bolded. **(c)** Structure of rOpx-H_6 with a linker (shaded) and the thrombin cleavage site sequence. **(d)** Structure of rOpx after cleavage of the H_6-tag with thrombin.

Figure S3. Three-dimensional structural model of nOpx obtained through the I-TASSER on-line server. The four HX-repeats are indicated by 1-4; N and C show N- and C-termini.The nOpx structure is most similar to plant PA2 albumins from *Vigna unguiculata* (PDB ID: 3OYO) [9] with a RMSD of 1.18 Å, and *Lathyrus sativus* (PDB ID: 3LP9) [8] with a RMSD of 1.20 Å.

Figure S4. Sensorgrams of rOpx interactions with cadaverine, putrescine, spermidine, and spermine (all 2 mM in phosphate buffered saline, pH 7.4). Polyamines were injected over rOpx that was immobilized on the CM5 chip, at a flow rate of 30 µL/min for 60 s, at 25 °C. Sensorgrams were corrected for reference flow-cell response.

Figure S1

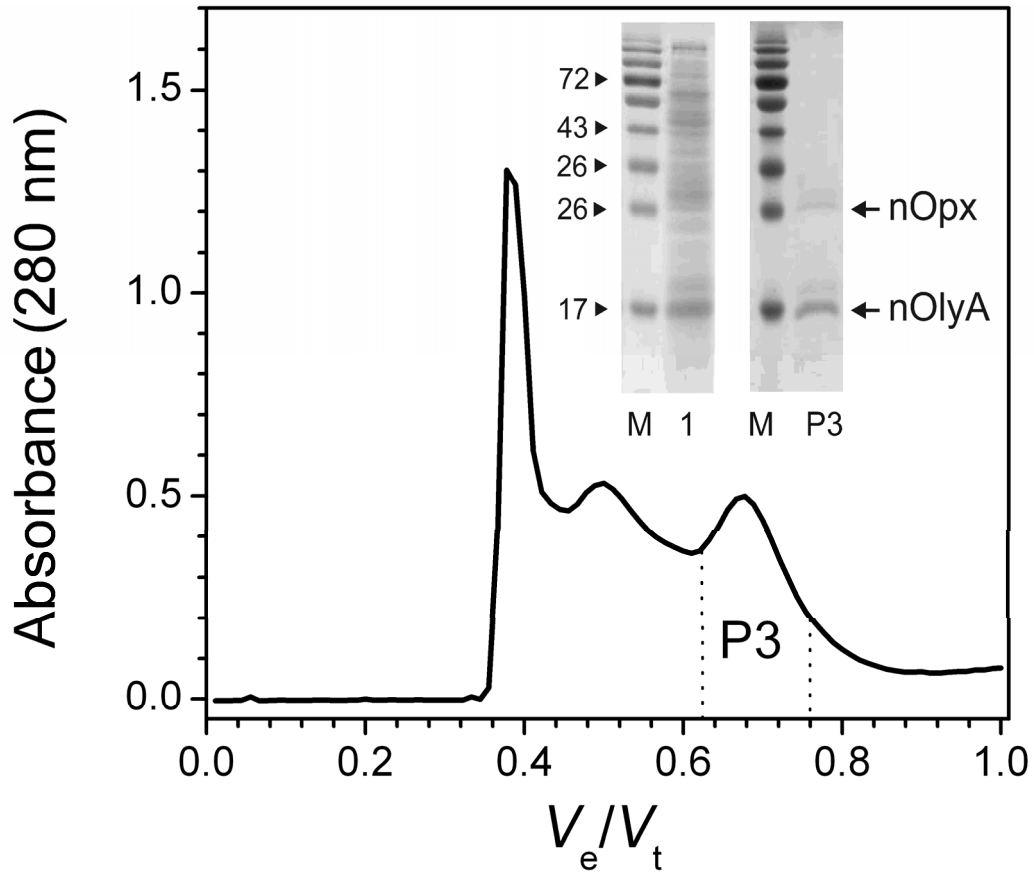
Absorbance (280 nm)
1.5
1.0
0.5
0.0
0.0
0.2
0.4
0.6
0.8
1.0
V_e/V_t
P3
72
43
26
26
17
nOpx
nOlyA
M
1
M
P3

Figure S2

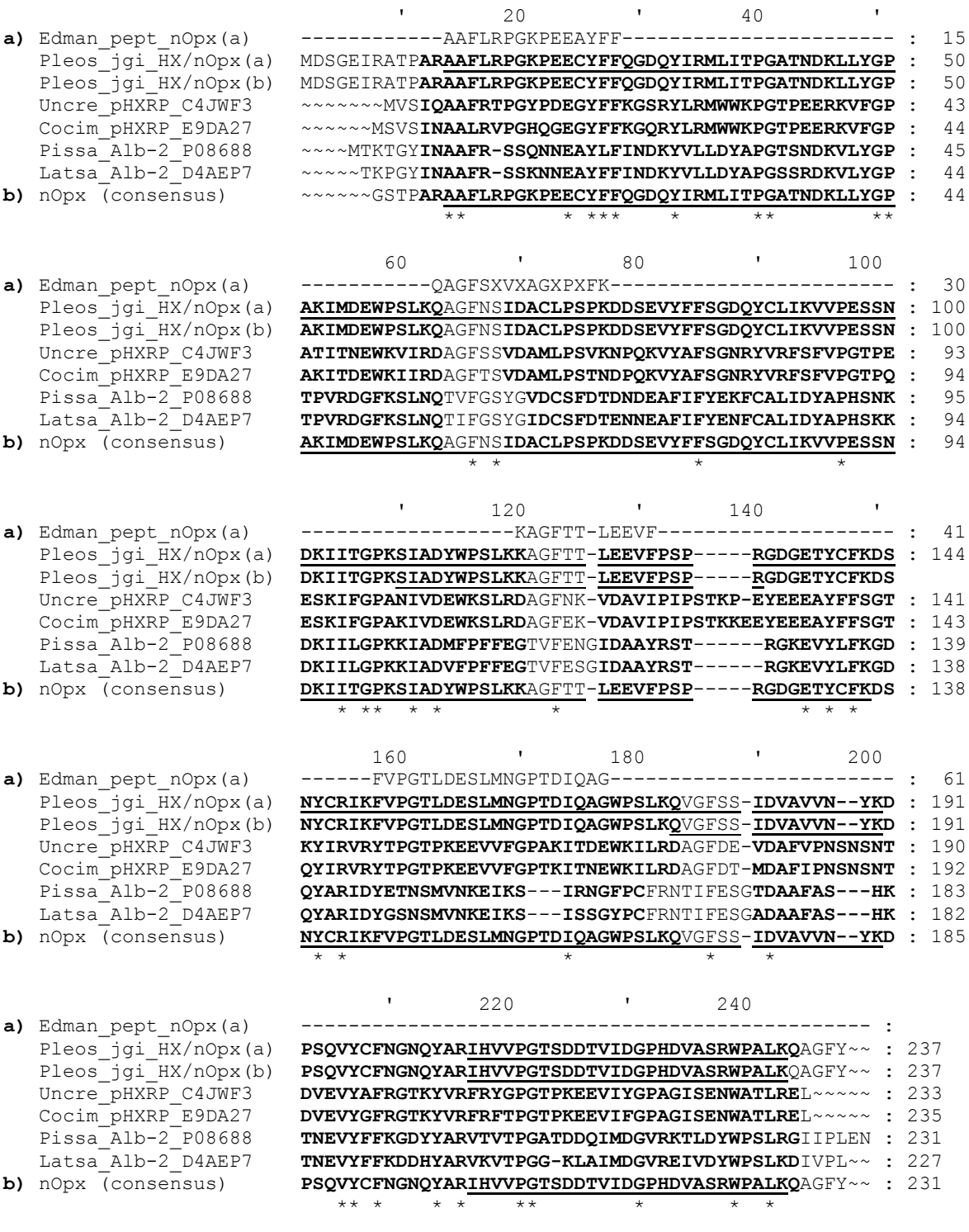

c) rOpx-H_6 = consensus nOpx-GSEGKSSGLVPRGSHHHHHH
d) rOpx = nOpx-GSEGKSSGLVPR

Figure S3

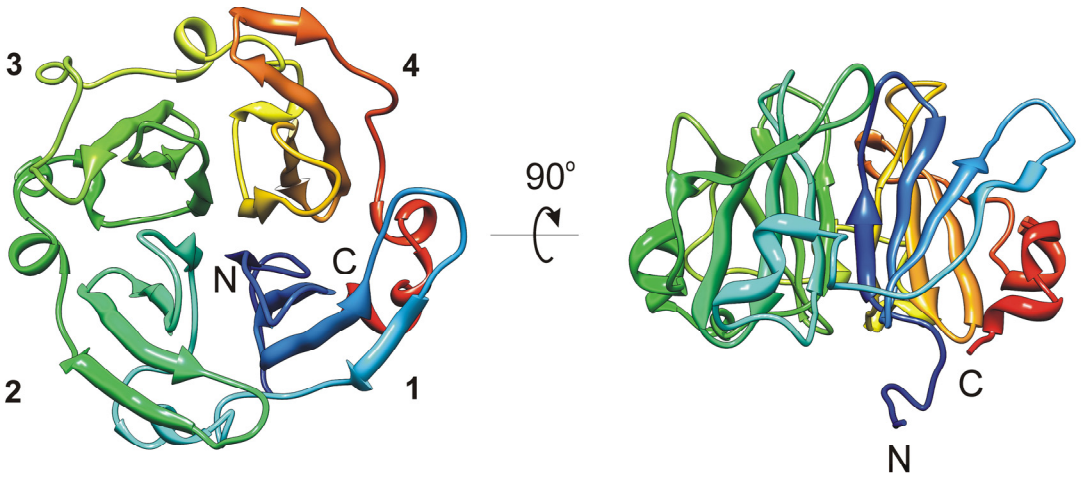

Figure S4

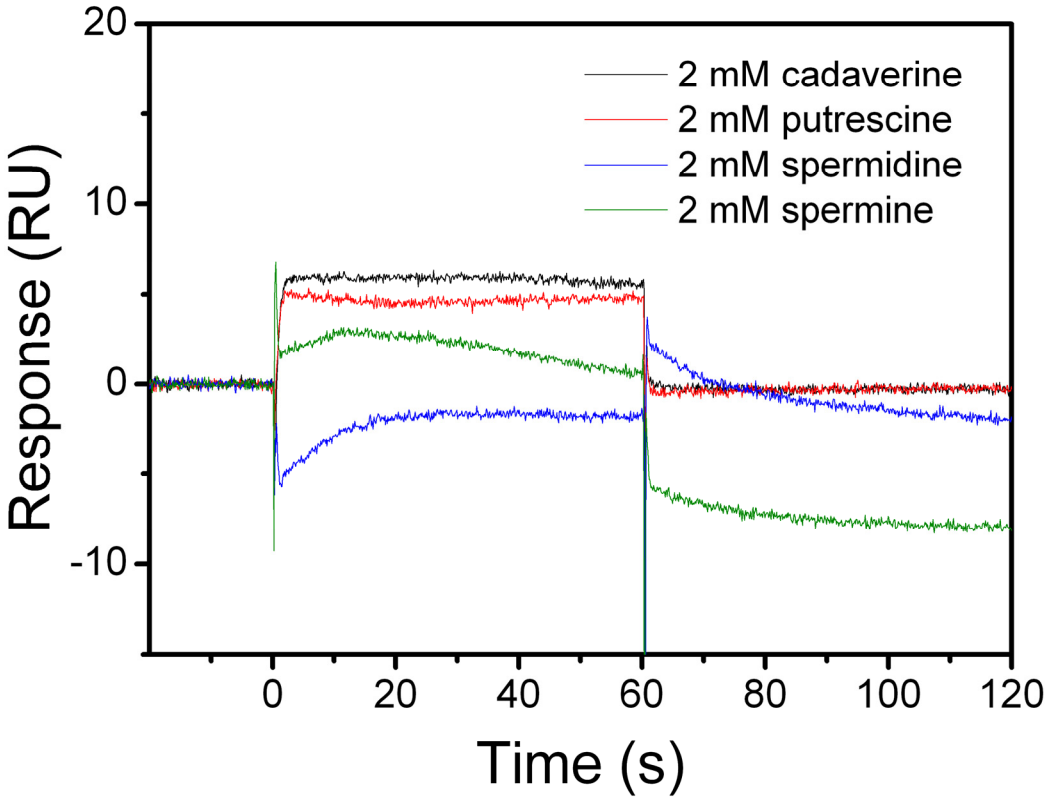
20
10
0
-10
Response (RU)
0
20
40
60
80
100
120
Time (s)
2 mM cadaverine
2 mM putrescine
2 mM spermidine
2 mM spermine